Supplementary information

SEM of hydrates
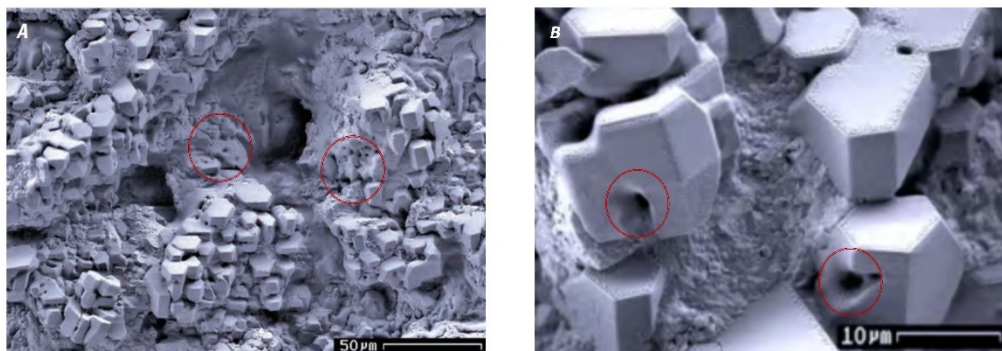
Figure S1 U.S. Energy Information Administration, In situ SEM of hydrates published in 2017 [1,2]:
(A) Undersea hydrate in the Gulf of Mexico; (B) Undersea hydrate in the Indian Ocean (Obvious holes are observed on the hydrate surface, most likely caused by nano-bubble rupture impacts.)

System construction

To investigate the changes in the material state in the local area during nanobubble rupture, we have constructed a structural model of methane nanobubbles surrounded by water, as illustrated in Figure 1(a). The simulated box size is 20 nm × 20 nm × 40 nm, with the central section shown in Figure 1(a) having a thickness of 2 nm. The upper 10 nm region is the vacuum layer, while the lower 30 nm region comprises the impact layer (2 nm), the movable part (nanobubble and water coexistence region), and the fixed layer (2 nm). In order to simulate the crystal growth process of natural gas hydrate, we have employed a type I natural gas hydrate model [3] to construct the structure shown in Figure 1(b). The studied system size is 6.97 nm × 6.97 nm × 6.97 nm, containing 1472 methane molecules and 9936 water molecules. The methane molecules are represented by red particles, while the O and H atoms in the water molecules are represented by yellow and white particles, respectively.
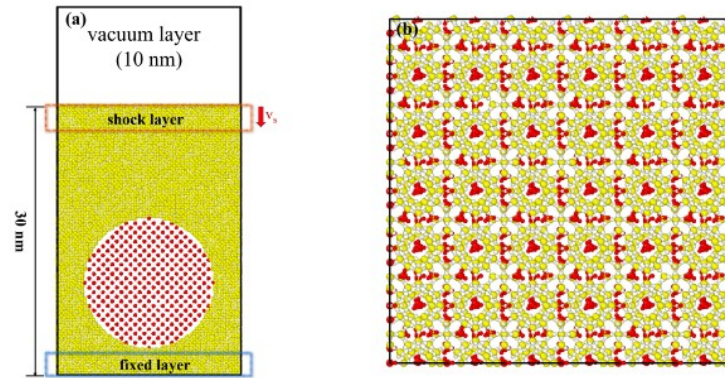
Figure S2 Main simulation initial model:(a) The initial model for impact-induced nanobubble rupture; (b) The model for a 6×6×6 pure hydrate.

Force fields and simulation details

To conduct the simulations, we employed the LAMMPS molecular dynamics software package developed by Sandia Laboratories in the United States [4]. We used periodic boundary conditions, the OPLS-UA force field [5] to describe the force field of methane, and the SPC force field to model water molecules. We applied a truncation radius of 1.5 nm for both Van der Waals and Coulomb interactions and used a time step of 1 fs to control the temperature and pressure of the system by Berendsen [6]. To maintain the rigidity of water, we utilized a dithering algorithm [7]. The interaction parameters between atoms are presented in Table 1. From the figure S3, it can be seen that at the moment of the nanobubble rupture, the atomic velocities at the six typical positions have increased significantly, and the closer to the bottom, the greater the effect of the shock, the more obvious the change.

Table S1 Atom pair interaction parameters.

Atom pairs	σ/Å	ε/(eV)
Cm-Hm	4.0000	0.0020810
Cm-Cm	3.5000	0.0028620
Hw-Hw	0.0000	0.0000000
Hw-Hm	1.5000	0.0013010
Hw-Cm	2.2000	0.0019300
Hm-Hm	4.5000	0.0013000
Ow-Ow	3.1656	0.0067366
Ow-Hw	0.0000	0.0000000
Ow-Cm	3.6270	0.0052910
Ow-Hm	2.7770	0.0035150
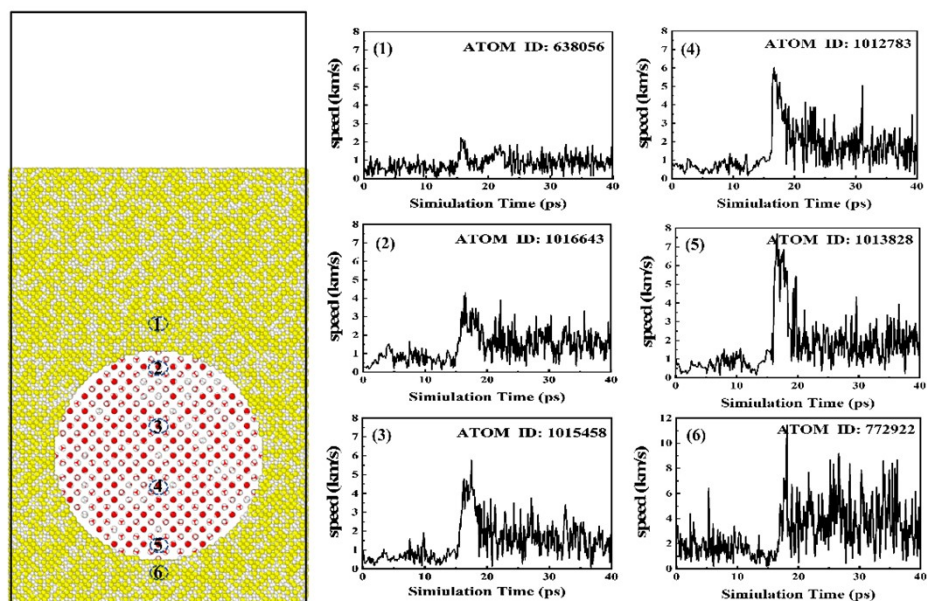
Figure S3 (1-6) Velocity transformation diagrams of atoms at different locations for nanobubble rupture (the left panel indicates the location of the selected atoms).

Data from other calculation groups

F_3 Order parameter

For hydrates, the values for the intact type I hydrate F3 are 0.01 and F4 is 0.89. Combined with Figures S4 to S7, it can be found that hydrate formation is not effective when the temperature is greater than 300 K. And for the high-pressure group (20000 bar and 40000 bar), too high pressure can deform the cage structure of hydrate, which is not favorable to the formation of hydrate structure. This part of the data shows: in the process of hydrate formation, as the external pressure becomes larger and larger, there will be a limited pressure, when the hydrate structure can be formed. The optimum pressure is reached when hydrate structures are most easily formed (the best results are available for 250 K and 100 Mpa). After that, the higher the pressure, the more unfavorable the hydrate formation is. And the effect of temperature on hydrate formation is that the higher the temperature is, the more unfavorable the hydrate formation is.
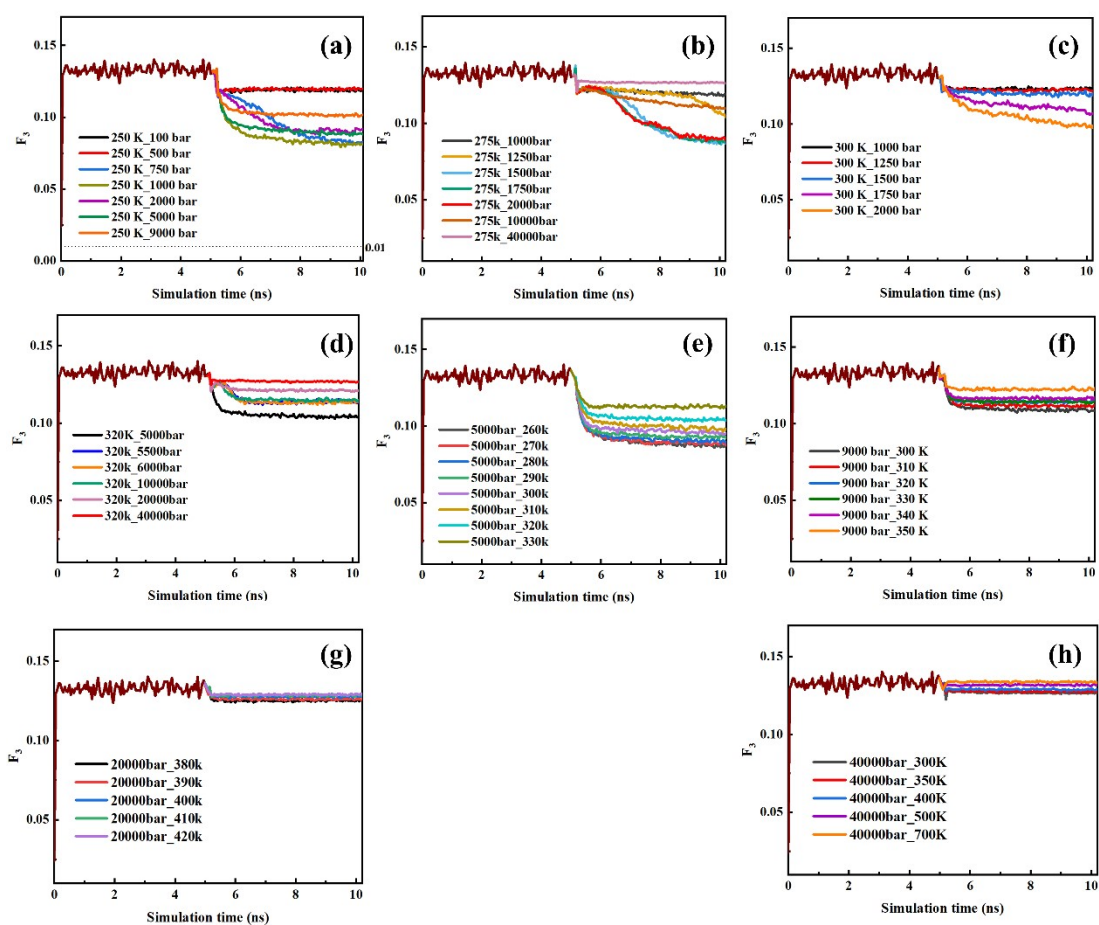
Figure S4 Other computational groups of F_3 Order parameter.

F$_4$ Order parameter
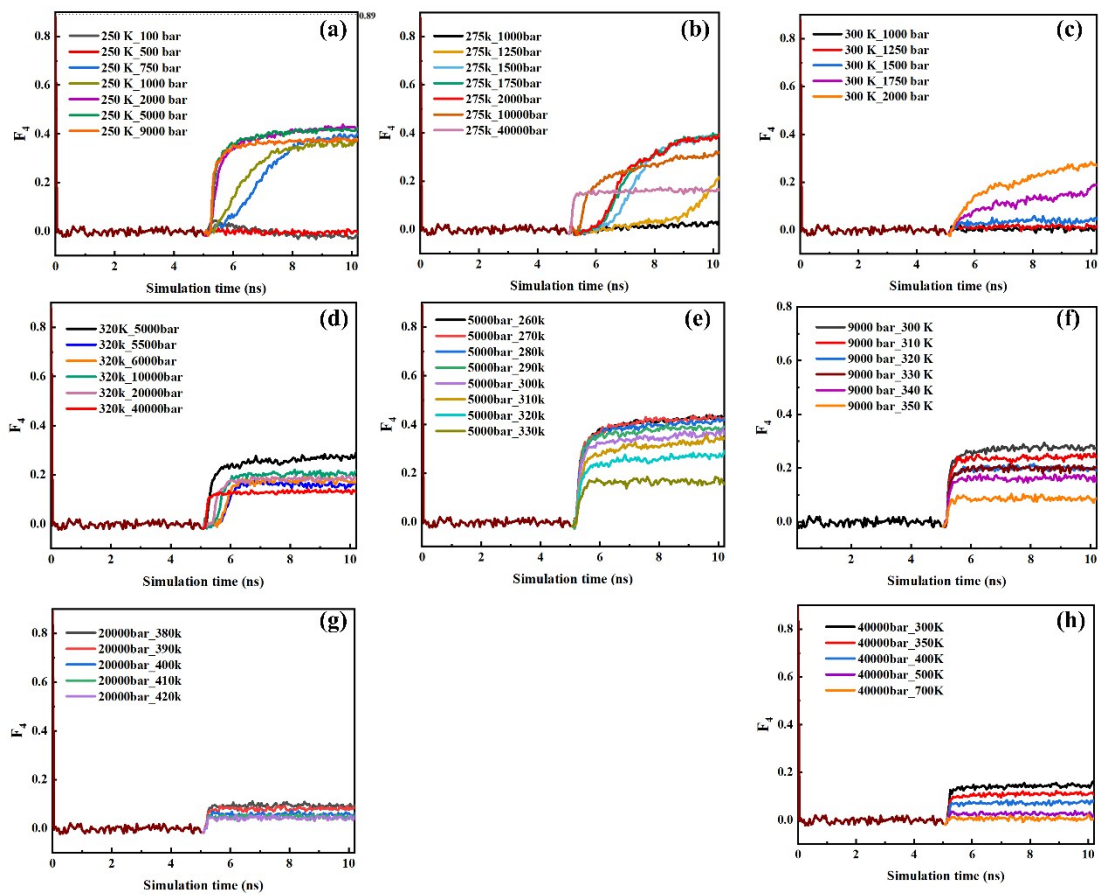
Figure S5 Other computational groups of F$_4$ Order parameter.

Number of 5¹² small cages
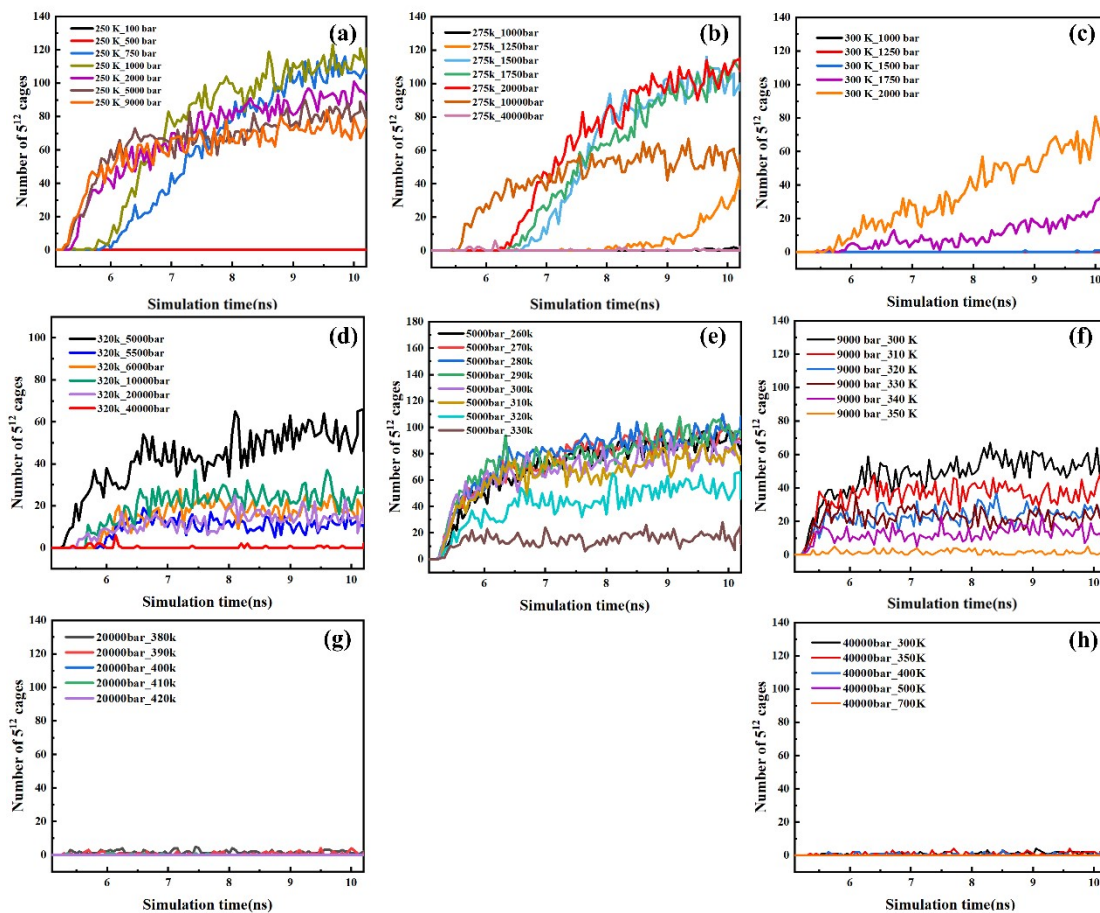
Figure S6 Number of 5^{12} small cages in other calculation groups.

Number of $6^2 5^{12}$ large cages
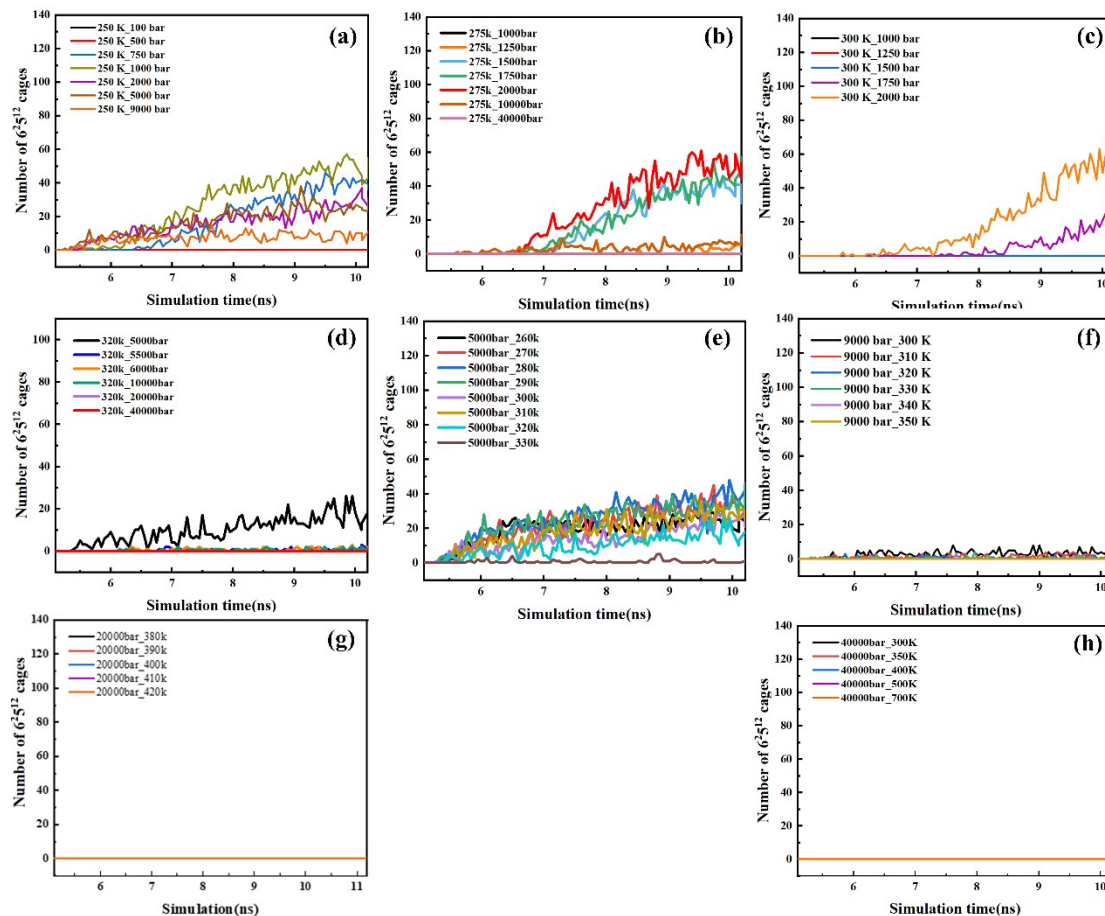
Figure S7 Number of $6^2 5^{12}$ large cages in other calculation groups.

Radial distribution functions and XRD
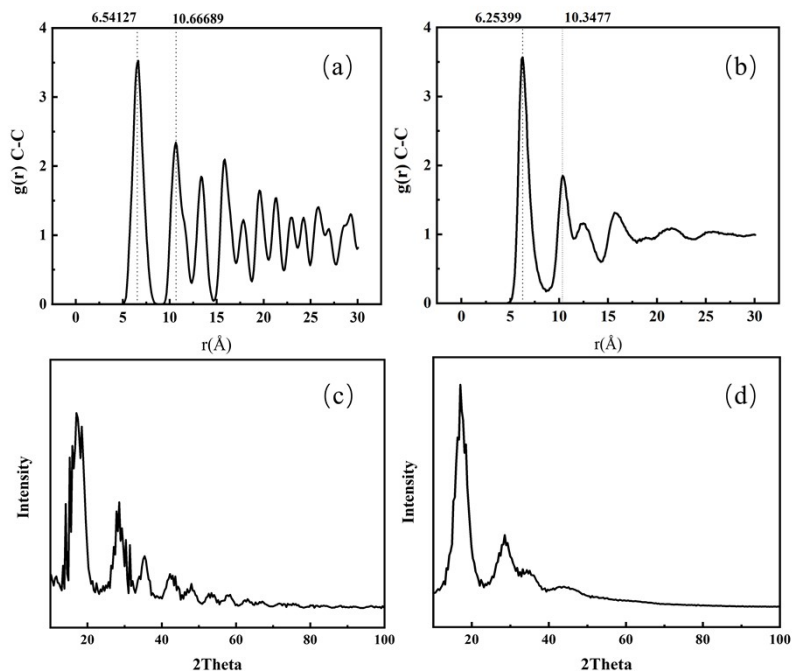
Figure S8 (a-b) Radial distribution functions of the structure of intact type I methane hydrate and the structure of the system after cooling down for 5 ns；(c-d) XRD of the intact type I methane hydrate structure and the system structure after cooling down for 5 ns (250 K,1000 bar). It indicates that hydrate structures are generated in the simulated system.
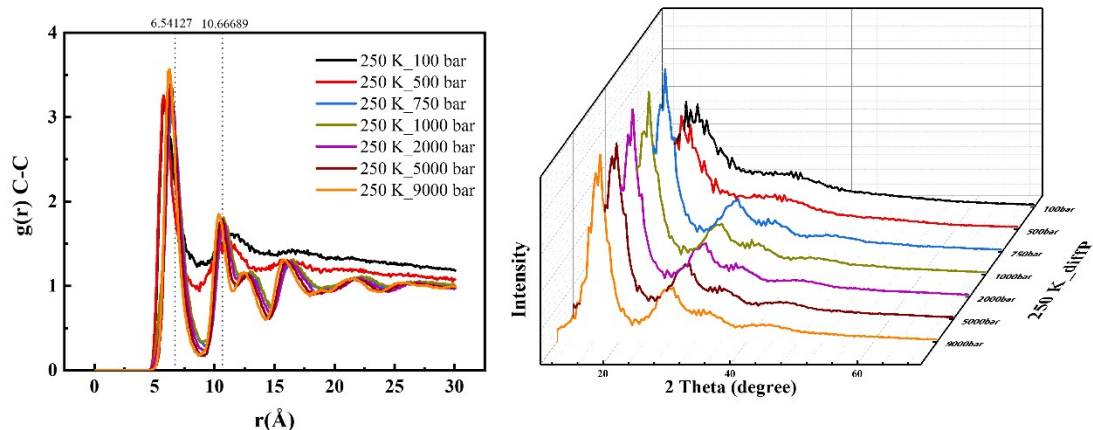
Figure S9 Radial distribution functions and XRD for different pressure groups at 250 K:(a) plots of radial distribution function at different temperatures at 5 ns after cooling; (b) XRD at different temperatures at 5 ns after cooling (It is deduced that the ultimate pressure of 250 K is between 500 bar and 750 bar).

Data for 300 ~350 K at 9000 bar
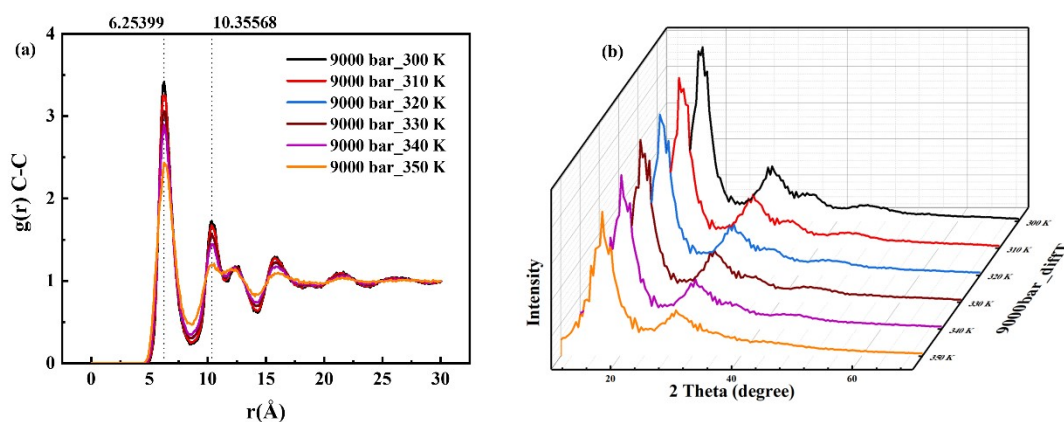
Figure S10 Plots of the radial distribution function and XRD results at 9000 bar: (a) plots of radial distribution function at different temperatures at 5 ns after cooling; (b) XRD at different temperatures at 5 ns after cooling (This indicates that the increase in temperature is detrimental to the hydrate generation situation).
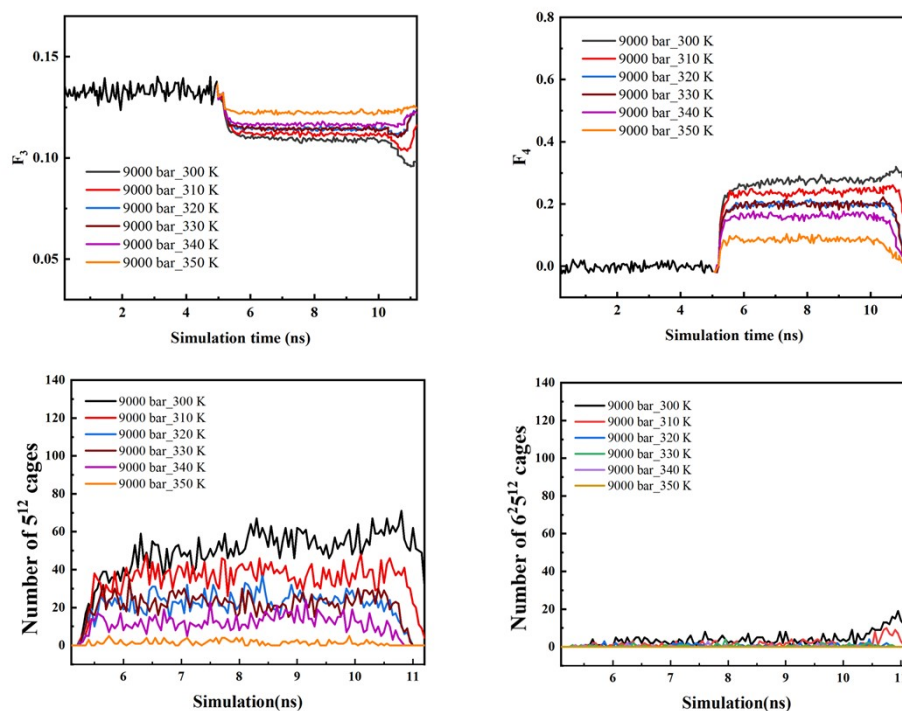
Figure S11 (a) Trend diagram of F_3 at different temperatures at 9000 bar; (b) Trend diagram of F_4 at different temperatures at 9000 bar; (c) Trend diagram of 5^{12} small cages at different temperatures at 9000 bar; (d) Trend diagram of $6^2 5^{12}$ small cages at different temperatures at 9000 bar (Combined with g(r) and XRD results, it shows that the hydrate formation is not good under the external environment of 350 K).

Data for the last model
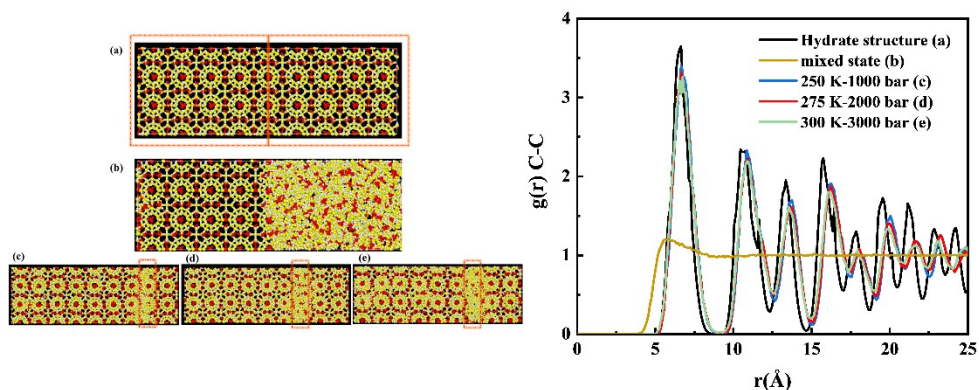
Figure S12 The right figure is the radial distribution function of the structure of the left figure (a~e) (both are taken from the right unfixed area). It shows that hydrates are formed in the system at all three temperature-pressure environments.

1   Ruppel, C. D. The U.S. Geological Survey's Gas Hydrates Project. doi:10.3133/fs20173079 (2018).

2   Ruppel, C. D. Gas hydrate in nature. doi:10.3133/fs20173080 (2018).

3   McMullan, R. K. & Jeffrey, G. A. Polyhedral Clathrate Hydrates. IX. Structure of Ethylene Oxide Hydrate. *The Journal of Chemical Physics* **42**, 2725-2732, doi:10.1063/1.1703228 (1965).

4   Plimpton, S. Fast Parallel Algorithms for Short-Range Molecular Dynamics. *Journal of Computational Physics* **117**, 1-19, doi:10.1006/jcph.1995.1039 (1995).

5   Jorgensen, W. L. & Tirado-Rives, J. The OPLS [optimized potentials for liquid simulations] potential functions for proteins, energy minimizations for crystals of cyclic peptides and crambin. *J Am Chem Soc* **110**, 1657-1666, doi:10.1021/ja00214a001 (1988).

6   Berendsen, H. J. C., Postma, J. P. M., van Gunsteren, W. F., DiNola, A. & Haak, J. R. Molecular dynamics with coupling to an external bath. *The Journal of Chemical Physics* **81**, 3684-3690, doi:10.1063/1.448118 (1984).

7   Ryckaert, J.-P., Ciccotti, G. & Berendsen, H. J. C. Numerical integration of the cartesian equations of motion of a system with constraints: molecular dynamics of n-alkanes. *Journal of Computational Physics* **23**, 327-341, doi:10.1016/0021-9991(77)90098-5 (1977).